Journal of the Mechanical Behavior of Biomedical Materials 93 (2019) 70–80

Contents lists available at ScienceDirect

Journal of the Mechanical Behavior of Biomedical Materials

journal homepage: www.elsevier.com/locate/jmbbm

Theoretical analysis of nanoshell-assisted thermal treatment for subcutaneous tumor

Jingxuan Ma[a], Xianfeng Yang[a], Yuxin Sun[a,*], Jialing Yang[a], Jilin Yu[b]

[a] Institute of Solid Mechanics, School of Aeronautic Science and Engineering, Beihang University, Beijing 100191, PR China
[b] CAS Key Laboratory of Mechanical Behavior and Design of Materials, University of Science and Technology of China, Hefei, Anhui 230027, PR China

ARTICLE INFO

Keywords:
Living bio-tissue
Thermal treatment
Green's function method
Thermal damage
Multi-layered structure

ABSTRACT

The hyperthermia is an efficient technique for tumor treatment, in which the tumor is subjected to a heating source, such as laser, supersonic or electromagnetic field. In order to improve the therapeutic efficiency and to protect the surrounding healthy tissues, gold nanoshells are embedded in the tumor as the additive to make it absorb more thermal energy than the healthy tissues. In the present study, a one-dimensional three-layered model is established to investigate the thermal response of the bio-tissue in the hyperthermia treatment for subcutaneous tumor. The governing equations are solved analytically by using the Green's function method and the Henriques' model is employed to evaluate the degree of thermal damage in the target tissue. The influences of the volumetric density of gold nanoshells on the temperature distribution and thermal damage are discussed in detail. When the gold nanoshells are embedded with a proper density, it can improve the efficiency of tumor killing and protecting the subcutaneous tissue from being burnt. The closed-form solution for the governing equations in multilayered tissues can be a theoretical guideline to selection of appropriate parameters of the gold nanoshells.

1. Introduction

Hyperthermia has become a significant and efficient therapeutic method for tumor treatment. The tumor cells are more sensitive to the high temperature than the healthy cells. The temperature of 41–47 ℃ will cause irreversible damage in the cancer cells by loosening the cell membranes and denaturing the proteins (Huang et al., 2008). The heating sources include the radio frequency, microwaves and ultrasound waves. However, these sources suffer from the drawbacks of the associated damage to the surrounding healthy tissues. An alternative strategy is photothermal therapy (PTT) in which photothermal agent is employed for heat generation in a local environment (Huang et al., 2016). Laser beam is a suitable heating source because of the high parallelism degree, energy concentration and reliability. To ensure the patients' safety and improve treatment efficiency in laser hyperthermia, one of the most significant issues is to predict the thermal response of the bio-tissue induced by laser beam. The interaction between the heating source and vivo bio-tissue in thermal therapy has attracted much attention of researchers. Among them, Lin and Li (2016) analytically investigated bioheat transfer and heat-induced mechanical response in bi-layered human skin with variable thermal material properties. Cercadillo-Ibarguren et al. (2010) carried out an experimental study to perform a histological evaluation of the thermal effect produced on soft tissue irradiated with CO_2, Er, Cr:YSGG or diode lasers. It was found that the wave length of the laser determines the absorption rate characteristics of every tissue and the thermal effect. Tuncer et al. (2010) compared the conventional surgery with CO_2 laser operative on oral soft tissue pathologies and proved that CO_2 laser was an effective instrument for soft tissue excisional biopsies with minimal intraoperative and postoperative complications and good pain control.

Heat transport in biological tissues is complicated due to the effects of the vascular system, blood-tissue convection, blood perfusion, and metabolic heat generation. The accurate description of the temperature distribution in tissues is critical to preclude thermal damage in thermotherapy. The first research to investigate the thermal response of bio-tissue was made by Pennes (1948) who developed a bio-heat transfer model for living tissues by combining the Fourier's law with the effects of metabolism and blood vascular system. The Pennes model has been successfully utilized in a batch of researches. For example, Shih et al. (2007) and Hooshmand et al. (2015) investigated the effects of the thermal response of a semi-infinite biological tissue due to a sinusoidal heat flux at the skin. Shih et al. (2007) and Hooshmand et al. (2015) studied the bioheat transfer behaviors of biological tissues induced by laser irradiation. Cui et al. (2016) presented an analytical heat transfer

* Corresponding author.
E-mail address: yxsun@buaa.edu.cn (Y. Sun).

https://doi.org/10.1016/j.jmbbm.2019.01.016
Received 18 October 2018; Received in revised form 24 January 2019; Accepted 28 January 2019
Available online 01 February 2019
1751-6161/

model for targeted brain hypothermia based on Pennes model. Yue et al. (2004) developed a one-dimensional steady-state bio-heat transfer model of living tissues in cylindrical coordinates. Dai et al. (2004) developed a fourth-order compact finite-difference scheme for solving the one-dimensional Pennes bioheat transfer equation in a triple layered skin structure. (Malek and Abbasi, 2016) derived the analytical and mild solutions of Pennes boundary control problem, which yields a discrete optimization problem for temperature profile at the specific depth point as well as temperature profile in the skin at the final time. Ezzat et al. (2014) developed a new mathematical model for Pennes bioheat equation with the usage of fractional calculus and investigated the thermal behaviors in vivo tissue which was subjected to instantaneous surface heating.

The safety of patients is the most significant requirement in the thermal therapy, so a lot of researches were focused on the thermal damage of bio-tissues. Liu et al. (2012) proposed that skin damage could be represented as a chemical rate process, which could be calculated by using a first order Arrhenius rate equation, whereby damage is related to the rate of protein denaturation and exposure time at a given absolute temperature. Based on this theory, Verma et al. (2017) studied biothermomechanics of skin tissues for one-dimensional and three-dimensional models. Liu et al. (2012) estimated the thermal damage in the living bio-tissue during the laser hyperthermia process by considering the non-Fourier effects of heat conduction. Verma et al. (2017) investigated the heat transfer characteristics in laser-skin-tumor-tissue interaction. A three-layered model was established and a finite volume based numerical bioheat transfer model was employed to predict the damage in healthy tissue. Kumar and Rai (2016) proposed a mathematical model on heat transfer in multilayered tissues in finite domain to predict the control temperature profile at hyperthermia position. The finite element Legendra wavelet Galerkin approach was used to solve the governing equations. Afrin et al. (2012) explored the thermal damage induced by laser irradiation by carrying out a numerical simulation. Two heat conduction models, namely DPL model and Pennes model, were used to derive the temperature response and thermal damage and the results of the two models were compared.

Gold nanoparticles have found great usage in biomedical applications, especially in tumor therapy. The laser energy absorption of bio-tissue is weaker than the scattering effects (Vera and Bayazitoglu, 2009a). The embedding of nanoparticles can enhance the energy absorption of the media, which will cause a localized high-temperature and kill the tumor cells. Vera and Bayazitoglu (2009b) used a one-dimensional radiative transport model to calculate the collimated and diffuse components of incident radiation in a series of semi-infinite nanoshell-embedded slabs, which represents human tissue media. It was shown that adding too many nanoshells or increasing laser power can cause overheating in the entry region while leaving the rear region heated only by conduction, producing an undesirable temperature differential. Hatef et al. (2015) carried out a numerical analysis to investigate the photothermal response of gold nanoshells with the most common size in an aqueous medium for biomedical applications. Xu et al. (2011) numerically studied nanoparticle-assisted laser-induced interstitial thermotherapy for cancer treatment. It was found that the local enhancement in laser photon absorption induced by nanoparticles will greatly prompt tumor hyperthermia. Tjahjono and Bayazitoglu (2008) investigated the heating of a one-dimensional, conducting and radiative participating medium due to embedded absorbing and scattering nanoparticles. The finite difference explicit method was used to derive the temperature distribution in the slab. Liu et al. (2009) derived a semi-analytical solution for a one-dimensional heat conduction equation, which described the heating process induced by pulsed laser and continuous-wave laser.

Green's function approach is useful in solving partial differential Eqs. Vahidhosseini et al. (2016) and Sun et al. (2017). For example, Yen and Beck (2004) used the Green's function method to investigate the axisymmetric two-dimensional heat conduction behavior of a bi-layered circular plate during pulsed laser heating. Flint et al. (2018) carried out a semi-analytical solution for the transient temperature fields that were generated in a three dimensional solid body when it is subjected to moving heat sources. Ma et al. (2018) developed a general solution for the dual-phase-lag heat conduction equation in a two-dimensional finite medium by utilizing the Green's function approach. The Green's function method is quite general in that all non-homogeneous problems are handled in the same manner and the solutions are presented formally in a very compact form (Ma et al., 2017; Ozisik, 1980). The principal difficulty in the use of Green's function approach appears to be the determination of the appropriate Green's function for a given problem, because it depends on the type of coordinate system, the boundary conditions, and the extent of the region (i.e., finite, semi-infinite, or infinite). Many researchers have been devoted to determining the appropriate Green's functions. At present, there are mainly two methods to obtain a Green's function: the Laplace transform method with respect to time variable, and the variable separation technique (Ozisik, 1980).

In summary, the above mentioned literatures mainly carried out numerical simulations and it is still hard to obtain the analytical solution for the thermal response in the nanoshell-assisted tumor hyperthermia. To address this issue, an analytical research is carried out to investigate the thermal treatment of the subcutaneous tumors. Green's function method is used to solve the thermal transfer equation for the multilayered nanoparticle-embedded bio-tissue subjected to the laser beam. Moreover, the thermal damages in the tumor and the healthy tissue are evaluated based on the closed-form solution as well as the Henriques' model. The effects of the volumetric density of nanoparticles and the optical parameters of the healthy tissue, tumor and gold nanoparticles are discussed in detail.

2. Mathematical models

2.1. Bio-heat conduction model

Pennes model is employed in the present study, which considered the heat exchange between the tissue and the blood in the capillary bed. It is assumed that the blood enters the capillaries at an arterial temperature and exits at the local tissue temperature. The Pennes bioheat conduction equation based on Fourier's law yields (Pennes, 1948; Nobrega and Coelho, 2017):

$$\rho_t c_t \frac{\partial T}{\partial t} = \nabla\cdot(k\nabla T) + w_b\rho_b c_b(T_a - T) + Q_m + Q_{laser} \tag{1}$$

where, ρ_t represents the tissue density, c_t the tissue specific heat, T the tissue temperature, k the tissue heat conductivity, w_b the blood perfusion rate, ρ_b the blood density, c_b the blood specific heat, $T_a$the body and arterial blood temperature, Q_m the metabolic heat generation per unit time and volume and Q_{laser} the volumetric heat source due to the laser beam.

2.2. Thermal damage model

The study of burnt damage caused by a thermal source on a living tissue is complex and multidisciplinary, which depends on the power of the heat source and its duration. Moritz R (1947) proposed an expression for the denaturation process based on the first order approximation of the Arrhenius equation. The denaturation rate K is defined as:

$$K(T) = A\exp\left(-\frac{E_a}{RT}\right) \tag{2}$$

where, A is the tissue frequency factor, R the universal gas constant and

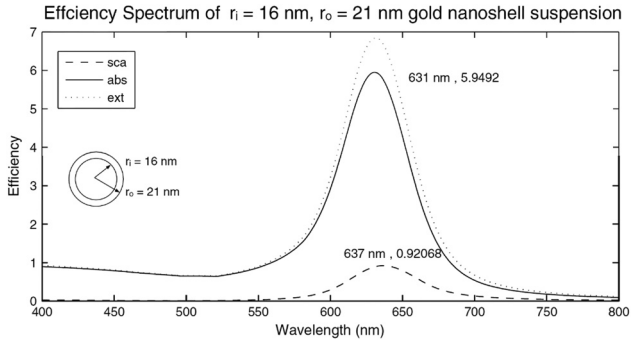

Fig. 1. Scattering and absorption spectra of the nanoshell suspension (Vera and Bayazitoglu, 2009a).

E_a the activation energy of the denaturation reaction. And the thermal damage can be evaluated as:

$$\Omega(t) = \int_0^t A \exp\left(-\frac{E_a}{RT}\right) dt \tag{3}$$

2.3. Energy absorption of nanoshells

The purpose of embedding nanoshells in the tumor is to augment the optical energy absorption of the tumor. According to the research of Vera and Bayazitoglu (2009a), the nanoshell with a core radius of 16 nm and shell thickness of 5 nm is a suitable choice with peak optical absorption and minimal scattering when exposed to a 633-nm laser, as shown in Fig. 1. The gold nanoshells are assumed to distribute uniformly in the tumor region.

The absorption coefficient for the nanoshell-embedded tumor can be derived from the summation of the absorption coefficients for tumor and nanoshells, which can be written as (Vera and Bayazitoglu, 2009a):

$$\mu_{20} = \mu_2 + \mu_0 \tag{4}$$

where, μ_2, μ_0 and μ_{20} are the absorption coefficients of the tumor, the nanoshell supplement and the nanoshell-embedded tumor.

The absorption coefficient for nanoshell supplement is determined by the geometry, optical characteristics ($Q_a = 5.9492\text{m}^{-1}$) and volume density of the nanoshells (N_T). In the present study, the absorption coefficient for nanoshell supplement can be calculated from the following formula (Vera and Bayazitoglu, 2009a):

$$\mu_0 = \pi r_0^2 Q_a N_T \tag{5}$$

2.4. Governing model

In the present study, the target tissue in the thermal therapy is considered as a finite domain, which is shown in Fig. 2. The bio-tissue is considered as a one-dimensional model consisting of the normal tissue ($x_2 < x \le x_3$), the nanoshell-embedded tumor ($x_1 < x \le x_2$) and the skin as top layer ($0 \le x < x_1$). The laser beam irradiates the target tissue on the top surface ($x = 0$), which is considered as a body heat source in the three-layer tissue. The thermal condition on the top surface is assumed to be natural convection (the environment temperature $T_e = 20^{\circ}\text{C}$) and the temperature on the bottom is taken as the body temperature $T_0 = 37^{\circ}\text{C}$.

It is assumed that the laser power is absorbed in the three layers and the heat source can be regarded as the volumetric heat generation in each layer, which can be expressed as (Orndorff et al., 2017; Tang et al., 2006):

$$q_1(x) = q_0(1 - R_a)\mu_1 \exp(-\mu_1 x),\ 0 \le x \le x_1 \tag{6}$$

$$q_2(x) = q_0(1 - R_a)\mu_{20} \exp[-\mu_1 x_1 - \mu_{20}(x - x_1)],\ x_1 < x \le x_2 \tag{7}$$

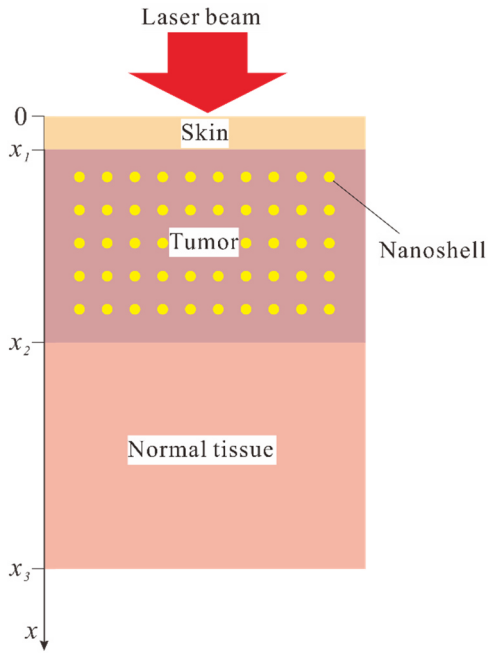

Fig. 2. Schematic geometry of the one-dimensional three-layered tissue.

$$q_3(x) = q_0(1 - R_a)\mu_3 \exp[-\mu_1 x_1 - \mu_{20}(x_2 - x_1) - \mu_3(x - x_2)],\ x_2 < x \le x_3 \tag{8}$$

where, q_0 is the energy density of the laser source, R_a the reflective ratio of each layer, and μ_1 and μ_3 the absorption coefficients of the first and the third layers, respectively.

With the Pennes model employed, the governing equations of the three-layered system can be written as:

$$\begin{cases} \rho_1 c_1 \frac{\partial \theta_1}{\partial t} = k_1 \frac{\partial^2 \theta_1}{\partial x^2} - w_{b1}\rho_b c_b \theta_1 + q_{m1} + q_1,\ 0 \le x \le x_1 \\ \rho_2 c_2 \frac{\partial \theta_2}{\partial t} = k_2 \frac{\partial^2 \theta_2}{\partial x^2} - w_{b2}\rho_b c_b \theta_2 + q_{m2} + q_2,\ x_1 < x \le x_2 \\ \rho_3 c_3 \frac{\partial \theta_3}{\partial t} = k_3 \frac{\partial^2 \theta_3}{\partial x^2} - w_{b3}\rho_b c_b \theta_3 + q_{m3} + q_3,\ x_2 < x \le x_3 \end{cases} \tag{9}$$

where, $\theta_i = T_i - T_0$, ρ_i, c_i, k_i, w_{bi} and q_{mi} ($i = 1, 2, 3$) are the temperature rise, the density, the specific heat capacity, the heat conductivity, the blood perfusion and the metabolic heat generation of each layer, respectively. The subscript i refers to each layer ($i = 1$ for the skin, $i = 2$ for the tumor and $i = 3$ for the normal tissue). q_i is the external heating source, which is defined by Eqs. (6)–(8).

As is mentioned above, the top surface is set to be naturally convective and the bottom keeps at a constant temperature T_0. The thermal contacts between the three layers are assumed to be perfect, which implies continuity of temperature at the interfaces. So the boundary conditions can be written as:

$$\begin{cases} -k_1 \frac{\partial \theta_1}{\partial x} + h_1 \theta_1 = -h_1(T_0 - T_e), & \text{at } x = 0 \\ \theta_1 = \theta_2, & \text{at } x = x_1 \\ k_1 \frac{\partial \theta_1}{\partial x} = k_2 \frac{\partial \theta_2}{\partial x}, & \text{at } x = x_1 \\ \theta_2 = \theta_3, & \text{at } x = x_2 \\ k_2 \frac{\partial \theta_2}{\partial x} = k_3 \frac{\partial \theta_3}{\partial x}, & \text{at } x = x_2 \\ \theta_3 = 0, & \text{at } x = x_3 \end{cases} \tag{10}$$

And the initial conditions are

$$\begin{cases} \theta_1 = \theta_2 = \theta_3 = 0, & \text{at } t = 0 \\ \frac{\partial \theta_1}{\partial t} = \frac{\partial \theta_2}{\partial t} = \frac{\partial \theta_3}{\partial t} = 0, & \text{at } t = 0 \end{cases} \tag{11}$$

3. Analytical solution of governing equations

The Green's Function method, which is on the basis of superposition principle and turns out to be effective to solve partial differential equations, is employed in this section to solve the governing equations analytically.

3.1. Determination of Green's function for the problem

To determine the desired Green's functions appropriate for the solution of the non-homogeneous heat conduction equations, it is required to consider the homogeneous version of the problem defined by Eq. (9) for the same region, which is given as:

$$\begin{cases} \frac{\partial \theta_1}{\partial t} = \alpha_1 \frac{\partial^2 \theta_1}{\partial x^2} - \alpha_1 \frac{A_{b1}}{k_1}\theta_1, & 0 \le x \le x_1 \\ \frac{\partial \theta_2}{\partial t} = \alpha_2 \frac{\partial^2 \theta_2}{\partial x^2} - \alpha_2 \frac{A_{b2}}{k_2}\theta_2, & x_1 < x \le x_2 \\ \frac{\partial \theta_3}{\partial t} = \alpha_3 \frac{\partial^2 \theta_3}{\partial x^2} - \alpha_3 \frac{A_{b3}}{k_3}\theta_3, & x_2 < x \le x_3 \end{cases} \tag{12}$$

where $\alpha_i = \frac{k_i}{\rho_i c_i}$ is the thermal diffusivity.

In the auxiliary problem, the general initial conditions can be set as:

$$\begin{cases} \theta_1 = F_1(x) \quad \text{at} \quad t = 0 \quad \text{in } 0 \le x \le x_1 \\ \theta_2 = F_2(x) \quad \text{at} \quad t = 0 \quad \text{in } x_1 < x \le x_2 \\ \theta_3 = F_3(x) \quad \text{at} \quad t = 0 \quad \text{in } x_2 < x \le x_3 \end{cases} \tag{13}$$

By means of the variables separation method, θ_i can be separated in the following form:

$$\theta_i = X_i(x)\Gamma(t), \quad (i = 1, 2, 3) \tag{14}$$

The functions $X_i(x)$ should satisfy the following equations:

$$\begin{cases} \frac{1}{X_1}\frac{d^2X_1}{dx^2} = -\xi^2, & 0 \le x \le x_1 \\ \frac{1}{X_2}\frac{d^2X_2}{dx^2} = -\gamma^2, & x_1 < x \le x_2 \\ \frac{1}{X_3}\frac{d^2X_3}{dx^2} = -\mu^2, & x_2 < x \le x_3 \end{cases} \tag{15}$$

And

$$\begin{cases} k_1 \frac{\partial X_1}{\partial x} = h_1 X_1, & \text{at} \quad x = 0 \\ X_1 = X_2, & \text{at} \quad x = x_1 \\ k_1 \frac{\partial X_1}{\partial x} = k_2 \frac{\partial X_2}{\partial x}, & \text{at} \quad x = x_1 \\ X_2 = X_3, & \text{at} \quad x = x_2 \\ k_2 \frac{\partial X_2}{\partial x} = k_3 \frac{\partial X_3}{\partial x}, & \text{at} \quad x = x_2 \\ X_3 = 0, & \text{at} \quad x = x_3 \end{cases} \tag{16}$$

The solution for $\Gamma(t)$ is obtained as:

$$\Gamma(t) = \exp(-\lambda^2 t) \tag{17}$$

where,

$$\lambda^2 = \alpha_1\left(\xi^2 + \frac{A_{b1}}{k_1}\right) = \alpha_2\left(\gamma^2 + \frac{A_{b2}}{k_2}\right) = \alpha_3\left(\mu^2 + \frac{A_{b3}}{k_3}\right) \tag{18}$$

The mode functions in x-direction can be obtained as:

$$\begin{cases} X_{1,m}(x) = A_{1,m}\cos(\xi_m x) + A_{2,m}\sin(\xi_m x), & 0 \le x \le x_1 \\ X_{2,m}(x) = B_{1,m}\cos(\gamma_m x) + B_{2,m}\sin(\gamma_m x), & x_1 < x \le x_2 \\ X_{3,m}(x) = C_{1,m}\cos(\mu_m x) + C_{2,m}\sin(\mu_m x), & x_2 < x \le x_3 \end{cases} \tag{19}$$

where the coefficients $A_{1,m}$, $A_{2,m}$, $B_{1,m}$, $B_{2,m}$, $C_{1,m}$ and $C_{2,m}$ can be determined from the following equations, which are obtained by substituting Eq. (19) into Eq. (16):

$$\begin{cases} h_1 A_1 - k_1 \xi_m A_2 = 0 \\ A_1\cos(\xi_m x_1) + A_2\sin(\xi_m x_1) - B_1\cos(\gamma_m x_1) - B_2\sin(\gamma_m x_1) = 0 \\ -A_1 k_1 \xi_m \sin(\xi_m x_1) + A_2 k_1 \xi_m \cos(\xi_m x_1) + B_1 k_2 \gamma_m \sin(\gamma_m x_1) \\ \qquad - B_2 k_2 \gamma_m \cos(\gamma_m x_1) = 0 \\ B_1\cos(\gamma_m x_2) + B_2\sin(\gamma_m x_2) - C_1\cos(\mu_m x_2) - C_2\sin(\mu_m x_2) = 0 \\ -B_1 k_2 \gamma_m \sin(\gamma_m x_2) + B_2 k_2 \gamma_m \cos(\gamma_m x_2) + C_1 k_3 \mu_m \sin(\mu_m x_2) \\ \qquad - C_2 k_3 \mu_m \cos(\mu_m x_2) = 0 \\ C_1\cos(\mu_m x_3) + C_2\sin(\mu_m x_3) = 0 \end{cases} \tag{20}$$

Since Eq. (20) has untrivial solutions, the eigenvalues ξ_m, γ_m and μ_m should satisfy the following equation:

$$\begin{vmatrix} h_1 & -k_1\xi_m & 0 & 0 & 0 & 0 \\ \cos(\xi_m x_1) & \sin(\xi_m x_1) & -\cos(\gamma_m x_1) & -\sin(\gamma_m x_1) & 0 & 0 \\ -k_1\xi_m \sin(\xi_m x_1) & k_1\xi_m \cos(\xi_m x_1) & k_2\gamma_m \sin(\gamma_m x_1) & -k_2\gamma_m \cos(\gamma_m x_1) & 0 & 0 \\ 0 & 0 & \cos(\gamma_m x_2) & \sin(\gamma_m x_2) & -\cos(\mu_m x_2) & -\sin(\mu_m x_2) \\ 0 & 0 & -k_2\gamma_m \sin(\gamma_m x_2) & k_2\gamma_m \cos(\gamma_m x_2) & k_3\mu_m \sin(\mu_m x_2) & -k_3\mu_m \cos(\mu_m x_2) \\ 0 & 0 & 0 & 0 & \cos(\mu_m x_3) & \sin(\mu_m x_3) \end{vmatrix} = 0 \tag{21}$$

The unknown coefficients in Eq. (19) can be derived as:

$$\begin{aligned} &\{A_{1,m} = 1 \\ &A_{2,m} = \frac{h_1}{k_1\xi_m} \\ &B_{1,m} = \frac{k_1\xi_m \sin(\gamma_m x_1)[A_{1,m}\sin(\xi_m x_1) - A_{2,m}\cos(\xi_m x_1)] + k_2\gamma_m \cos(\gamma_m x_1)[A_{1,m}\cos(\xi_m x_1) + A_{2,m}\sin(\xi_m x_1)]}{k_2\gamma_m} \\ &B_{2,m} = \frac{k_1\xi_m \cos(\gamma_m x_1)[-A_{1,m}\sin(\xi_m x_1) + A_{2,m}\cos(\xi_m x_1)] + k_2\gamma_m \sin(\gamma_m x_1)[A_{1,m}\cos(\xi_m x_1) + A_{2,m}\sin(\xi_m x_1)]}{k_2\gamma_m} \\ &C_{1,m} = -\frac{[B_{1,m}\cos(\gamma_m x_2) + B_{2,m}\sin(\gamma_m x_2)]\sin(\mu_m x_3)}{\sin[\mu_m(x_2 - x_3)]} \\ &C_{2,m} = \frac{[-B_{1,m}\cos(\gamma_m x_2) + B_{2,m}\sin(\gamma_m x_2)]\cos(\mu_m x_3)}{\sin[\mu_m(x_2 - x_3)]} \end{aligned} \tag{22}$$

From Eq. (18), the following equation can be attained:

$$\lambda_m{}^2 = \alpha_1\left(\xi_m^2 + \frac{A_{b1}}{k_1}\right) = \alpha_2\left(\gamma_m^2 + \frac{A_{b2}}{k_2}\right) = \alpha_3\left(\mu_m^2 + \frac{A_{b3}}{k_3}\right) \tag{23}$$

Combining the initial conditions Eq. (13) and the boundary conditions Eq. (16), the complete solutions for Eq. (12) can be determined as:

$$\theta_i(x, t) = \sum_{m=1}^{\infty} \frac{\Theta_m}{M_m} \exp(-\lambda_m^2 t) X_{i,m}(x), \quad i = 1, 2, 3 \tag{24}$$

where, with the value of x_0 set to be zero,

$$\Theta_m = \sum_{i=1}^{3} \frac{k_i}{\alpha_i} \int_{x'=x_{i-1}}^{x_i} X_{i,m}(x') F_i(x') dx' \tag{25}$$

$$M_m = \sum_{i=1}^{3} \frac{k_i}{\alpha_i} \int_{x_{i-1}}^{x_i} X_{i,m}^2(x) dx \tag{26}$$

According to Green's function method, the solutions can be expressed in terms of Green's function as:

$$\theta_i(x, t) = \sum_{j=1}^{3} \int_{x'=x_{j-1}}^{x_j} G_{i,j}(x, t|x', \tau)|_{\tau=0} F_j(x') dx', \; i = 1, 2, 3 \tag{27}$$

With the comparison between the two sets of solutions (Eqs. (23) and (26)), the Green's function for the homogeneous problem can be obtained as:

$$G_{i,j}(x, t|x', \tau)|_{\tau=0} = \sum_{m=1}^{\infty} \frac{1}{M_m} \frac{k_j}{\alpha_j} \exp(-\lambda_m^2 t) X_{i,m}(x) X_{j,m}(x') \tag{28}$$

where, $i, j = 1, 2, 3$.

Then replace t in Eq. (27) by $(t - \tau)$, and the desired Green's function for Eq. (9) can be obtained as:

$$G_{i,j}(x, t|x', \tau) = \sum_{m=1}^{\infty} \frac{1}{M_m} \frac{k_j}{\alpha_j} \exp[-\lambda_m^2 (t - \tau)] X_{i,m}(x) X_{j,m}(x') \tag{29}$$

3.2. Solution for non-homogeneous heat conduction equations

According to Green's function method, the solutions for Eqs. (9)–(11) are

$$\theta_i(x, t) = \sum_{j=1}^{3} \int_{\tau=0}^{t} \int_{x'=x_{j-1}}^{x_j} G_{i,j}(x, t|x', \tau) \left[\frac{\alpha_j}{k_j} Q_j(x', \tau)\right] dx' d\tau + \int_{\tau=0}^{t} \left[\frac{\alpha_i}{k_i} G_{i,1}(x, t|x', \tau)|_{x'=0} f_1(\tau)\right] d\tau \tag{30}$$

where, $Q_j(x', \tau)$ represents the heat source in the j^{th} layer and $f_1 = -h_1(T_0 - T_e)$ is the boundary condition on the top boundary.

In the present research, all the three layers are influenced by the laser beam, so the heat source can be expressed as:

$$\begin{cases} Q_1(x') = q_{m1} + q_1(x'), \; 0 \le x \le x_1 \\ Q_2(x') = q_{m2} + q_2(x'), \; x_1 < x \le x_2 \\ Q_3(x') = q_{m3} + q_3(x'), \; x_2 < x \le x_3 \end{cases} \tag{31}$$

Table 1
Optical parameters of laser beam.

Parameters	Values
q_0, Power density(W/m^3)	1×10^4
R_a, Energy rejection coefficient	0.024

Table 2
Thermal and optical parameters of living tissue.

Parameters	Blood	Skin	Tumor	Subcutis
Thermal conductivity (W/m K)	–	0.293	0.51	0.21
Density (kg/m^3)	1060	1100	1050	911
Specific heat (J/kg K)	3770	3150	3950	2348
Blood perfusion (s^{-1})	–	0.0016	0.007	0.0006
Metabolic heat Generation (W/m^3)	–	368.1	4000	464.6
Absorption coefficient (m^{-1})	–	180	180	180
Thickness (m)	–	0.001	0.004	0.005

Table 3
Parameters for thermal damage prediction.

Temperature range (°C)	E_a/R(K)	A, Frequency factor(s^{-1})
$T \le 55$	7.5×10^4	3.1×10^{98}
$T > 55$	3.54×10^4	5.0×10^{45}

Substitute Eqs. (28) and (31) into Eq. (30), and the temperature increments in the three layers can be obtained as:

$$\theta_i(x, t) = \sum_{m=1}^{\infty} \frac{H_m}{M_m} X_{i,m}(x) P(t) \text{in} x_{i-1} < x < x_i, \; i = 1, 2, 3 \tag{32}$$

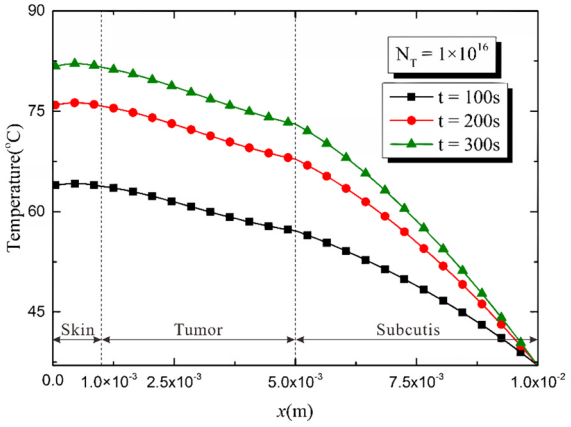

(a) Temperature along x-direction at different times.

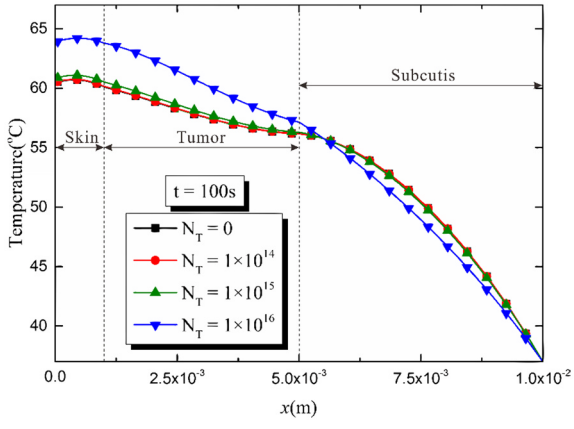

(b) Temperature along x-direction with different values of N_T.

Fig. 3. Temperature vs location in the target tissue.

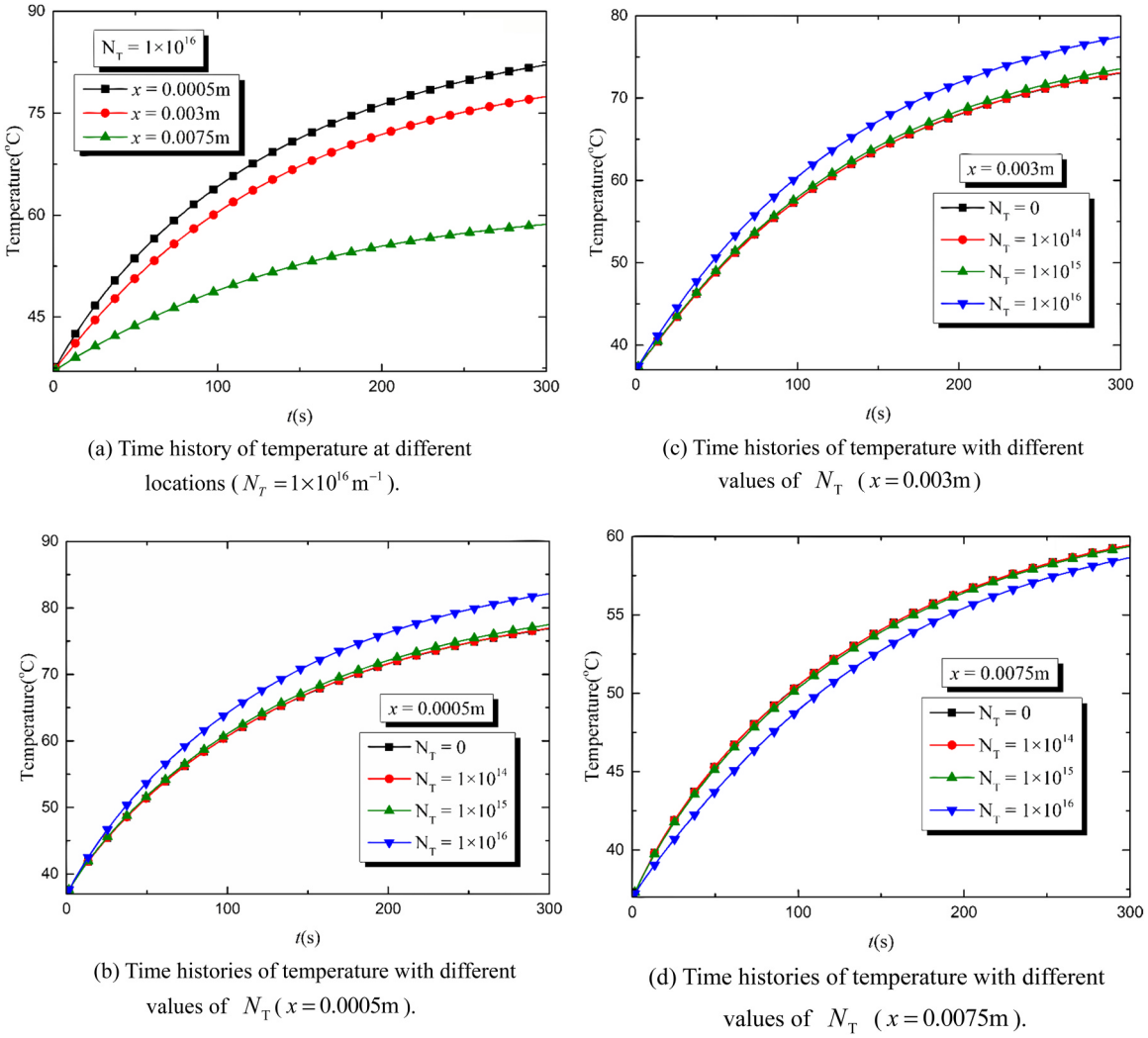

(a) Time history of temperature at different locations ($N_T = 1\times10^{16}\,\mathrm{m}^{-1}$).

(c) Time histories of temperature with different values of N_T ($x = 0.003\mathrm{m}$)

(b) Time histories of temperature with different values of N_T ($x = 0.0005\mathrm{m}$).

(d) Time histories of temperature with different values of N_T ($x = 0.0075\mathrm{m}$).

Fig. 4. Temperature variation with time.

where,

$$H_m = f_{1,m} + \sum_{i=1}^{3} (L_{i,m} + q_{mi} G_{i,m}) \tag{33}$$

$$G_{i,m} = \int_{x=x_{i-1}}^{x_i} X_{i,m}(x)dx \tag{34}$$

$$L_{i,m} = \int_{x_{i-1}}^{x_i} X_{i,m}(x) q_i(x)dx \tag{35}$$

$$P(t) = \int_0^t \exp[-\lambda_m^2 (t-\tau)]d\tau \tag{36}$$

4. Physical parameters

The physical parameters used in the present study are introduced in this section.

Table 4
Contribution of the nanoshells to the tumor's absorption coefficient.

Nanoshell density(m^{-1})	Nanoshell absorption coefficient(m^{-1})	Absorption coefficient of nanoshell embedded tumor(m^{-1})
1×10^{14}	0.824	180.824
1×10^{15}	8.24	188.24
1×10^{16}	82.4	262.4

The optical parameters of the laser beam which are introduced in Eqs. (6)–(8) are shown in Table 1. The heat sources are considered as volume heat sources in the three layers.

The thermal and optical parameters of the skin, tumor,

subcutaneous tissue and blood are shown in Table 2 (Vera and Bayazitoglu, 2009a; Nobrega and Coelho, 2017; Orndorff et al., 2017).

The parameters that characterize the thermal damage, which are introduced in Eqs. (2) and (3), are shown in Table 3 (Nobrega and Coelho, 2017). It is accepted that: $\Omega = 0.53$ represents the first-degree burn, $\Omega = 1$ for the second degree-burn and $\Omega = 10^4$ for the third-degree burn (Tzou, 1995; Lin, 2013).

5. Results and discussions

A calculating example for mathematical model in the present study is carried out with the usage of the physical parameters shown in Section 4. The central points of each layer ($x = 0.0005$ m, $x = 0.003$ m, $x = 0.0075$ m) are selected as typical points to represent the three layers respectively.

Fig. 3 shows the temperature variation with the x-coordinate in the target tissue during the laser treatment for tumor. It is shown in Fig. 3(a) that the peak value of the temperature appears below the top surface in the first layer (the skin). Due to the natural convection boundary condition, the temperature does not maximize at the top surface. The laser energy decays with the increasing of the depth, so the temperature decreases as well. With the time going by, the incident energy increases, and the bulk temperature of the target tissue rises. Fig. 3(b) shows the temperature distributions with the different nanoshell density. The embedding of nanoshells can augment the absorption coefficient of the tumor, as is shown in Eqs. (6)–(8). The temperature in the skin and the tumor increases with the increment of nanoshells density, however the temperature in the subcutis decreases. Especially, this phenomenon is obvious when the value of the density reaches $N_T = 1 \times 10^{16}\mathrm{m}^{-1}$, as is shown in Fig. 3(b). The participation of nanoshells changes the energy distribution in the target tissue. More energy is concentrated in the top layers and less energy is absorbed in the subcutaneous tissue. The increasing temperature-difference between the tumor and subcutis tissue due to the embedding of nanoshells was also found efficient for cancer therapy in the published literature (Vera and Bayazitoglu, 2009a).

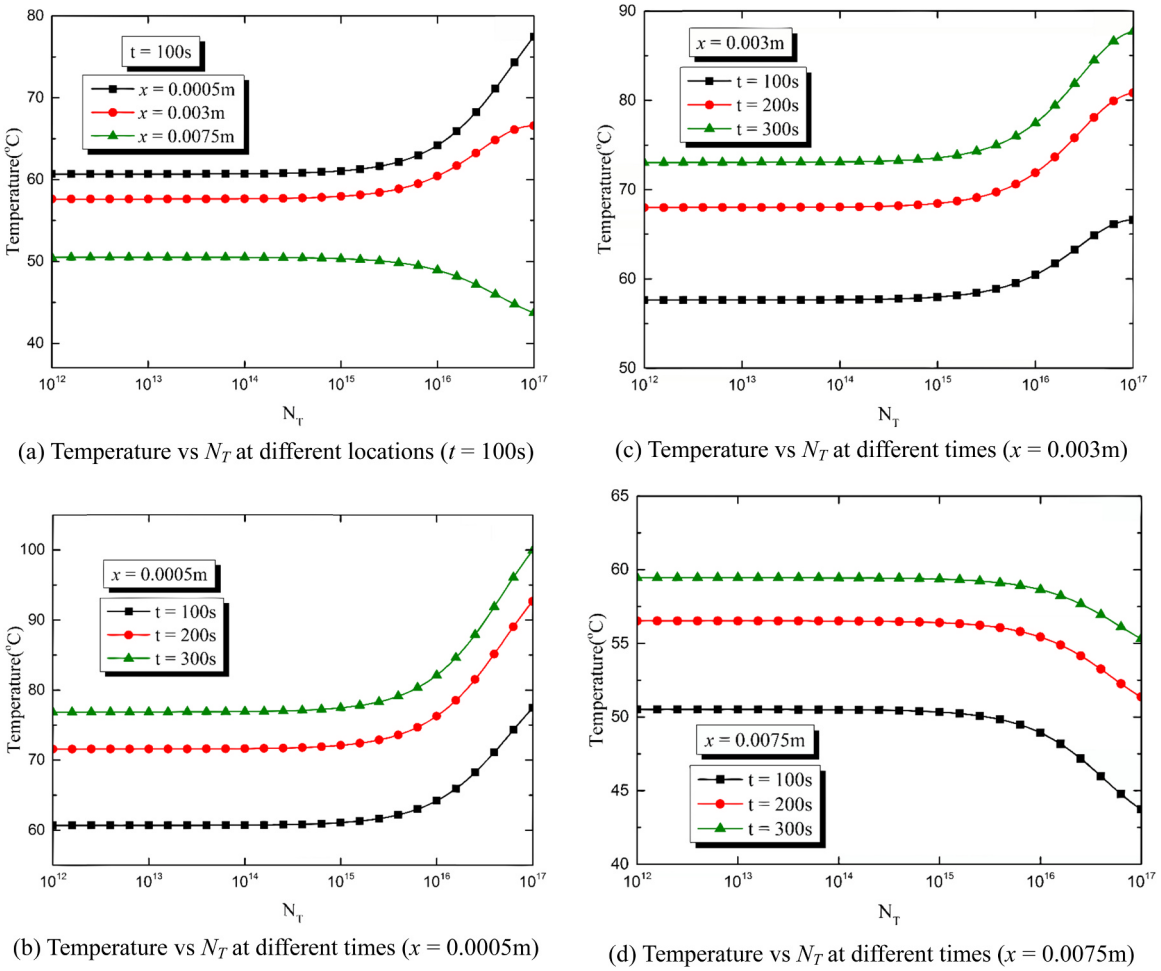

(a) Temperature vs N_T at different locations ($t = 100$s)

(c) Temperature vs N_T at different times ($x = 0.003$m)

(b) Temperature vs N_T at different times ($x = 0.0005$m)

(d) Temperature vs N_T at different times ($x = 0.0075$m)

Fig. 5. Temperature variation with the volumetric density of the gold nanoshells.

Fig. 4 shows the time histories of temperatures in the target tissue. The laser beam continues irradiating on the tissue, so the temperatures in the three layers increase with time going by. However, the temperature grows the fastest at the beginning and then slows down. The temperature drops down from layer to layer because of the optical extinction in the upper layer, as is shown in Fig. 4(a). Fig. 4(b) (c) and (d) show the temperature curves at a specified location in the skin, tumor and subcutis, respectively. As is introduced above, the embedding of nanoshells will enhance the energy absorption in the tumor and remain less energy for the subcutis. As a result, the temperature in tumor increases with the increment of nanoshell density, as is shown in Fig. 4(c). However, the thermal response in the subcutis is opposite to that in the tumor, as is shown in Fig. 4(d). The temperature in the subcutaneous tissue decreases due to the participation of the nanoshells, which was also mentioned in Vera's work (Vera and Bayazitoglu, 2009a). That is to say, the embedded nanoshells could advantage tumor hyperthermia in two aspects: optimizing the temperature distribution and shortening the treatment time. Table 4 shows the contribution of the nanoshells to the tumor's absorption coefficient. The absorption coefficient of the tumor without additive is $\mu_2 = 180\text{m}^{-1}$. With the comparison of μ_2 and the parameters presented in Table 4, it can be found that the absorption coefficient is obviously improved when the volumetric density of nanoshells reaches $N_T = 1 \times 10^{16}\text{m}^{-1}$, which agrees well with Fig. 4(b) (c) and (d).

It can be deduced that the gold nanoshells can offer excellent assistance in the tumor heat treatment by detaining more laser energy in the tumor instead of the subcutis. As a result, the increment of nanoshell density will raise the temperature of tumor and reduce the temperature of subcutaneous tissue. Fig. 5 shows the temperature variation with the volumetric density of the gold nanoshells.

It can be found from Fig. 5 that the gold nanoshells doesn't influence the temperature obviously until the volumetric density reaches the value of $N_T = 1 \times 10^{16}m^{-1}$. This influence becomes more and more significant with the increasing of N_T, which is in good agreement with Table 4. Fig. 5(a) shows the temperature curves at different positions in the target tissue. The points $x = 0.0005$ m, $x = 0.003$ m and $x = 0.0075$ m are located in the skin, the rumor and the subcutis, respectively, as has been mentioned above. It is clear that the increment of the nanoshell volumetric density leads to increasing of the tumor temperature and decreasing of the subcutaneous temperature. And this tendency becomes more and more noticeable with the increasing of nanoshell volumetric density. Fig. 5(b) (c) and (d) show the temperature curves at different time instants for each layer. It is shown in Fig. 5(b) and (c) that the temperatures of the skin and the tumor are in positive correlation with the radiation time and the volumetric density of nanoshells. However, the temperature of subcutaneous tissue is inversely proportional to the volumetric density of nanoshells, as is shown in Fig. 5(d).

In thermal treatment, it is demanded to protect the surrounding healthy tissues while killing the tumor cells. So it is necessary to study the thermal damage behavior of the tissue, which is determined by the temperature of the target tissue and it will be discussed in the following.

Fig. 6 shows the thermal damage of the target tissue caused by the laser radiation in the process of tumor heat treatment. Fig. 6(a) shows the thermal damage variation with x-coordinate at different times.

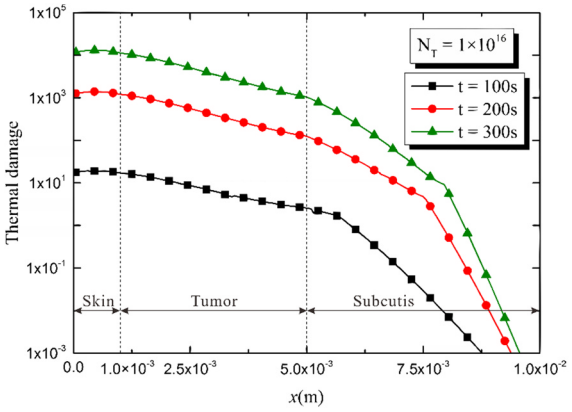

(a) Thermal damage along x -direction at different times.

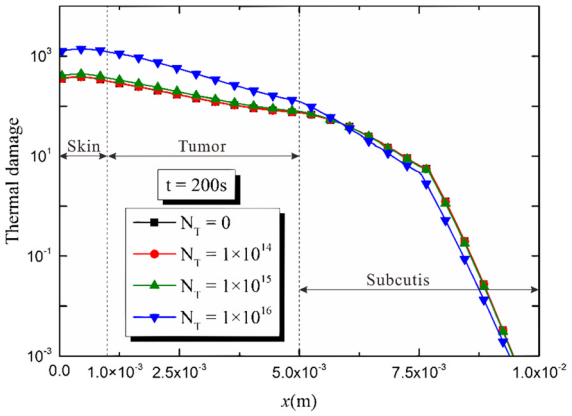

(b) Thermal damage along x -direction with different values of N_T .

Fig. 6. Thermal damage distributions in the target tissue.

The serious burn occurs mainly in the top two layers (the skin and the tumor). The degree of the burn decreases rapidly into the depth, because of the decreasing of the absorbed energy. Fig. 6(b) shows the influence of the nanoshell volumetric density on the thermal damage. Since more energy is absorbed by the tumor and less by the subcutaneous tissue due to the embedding of nanoshells, the burns in the skin and the tumor are deepened and the thermal damage in the subcutaneous tissue is weakened. That is to say, the nanoshell-assisted heat treatment will improve the curative effect for the tumor and protect the subcutaneous tissue from being seriously burnt meanwhile.

Fig. 7 shows the thermal damage in the target tissue, which varies with time. It is accepted that the irreversible damage occurs when $\Omega = 1$ (the second-degree burn), which corresponds to a denaturation of 63% of the molecules (Zhou et al., 2009). It is shown in Fig. 7(a) that the thermal damage in the three layers becomes more and more serious as time passes. However, the irreversible thermal damage occurs earlier in the skin and tumor than that in the subcutis. Fig. 7(b) (c) and (d) show the influences of the nanoshell embedding on the thermal damage in each layer. With the nanoshells embedded, the temperatures in the skin and tumor increase faster and higher. So the

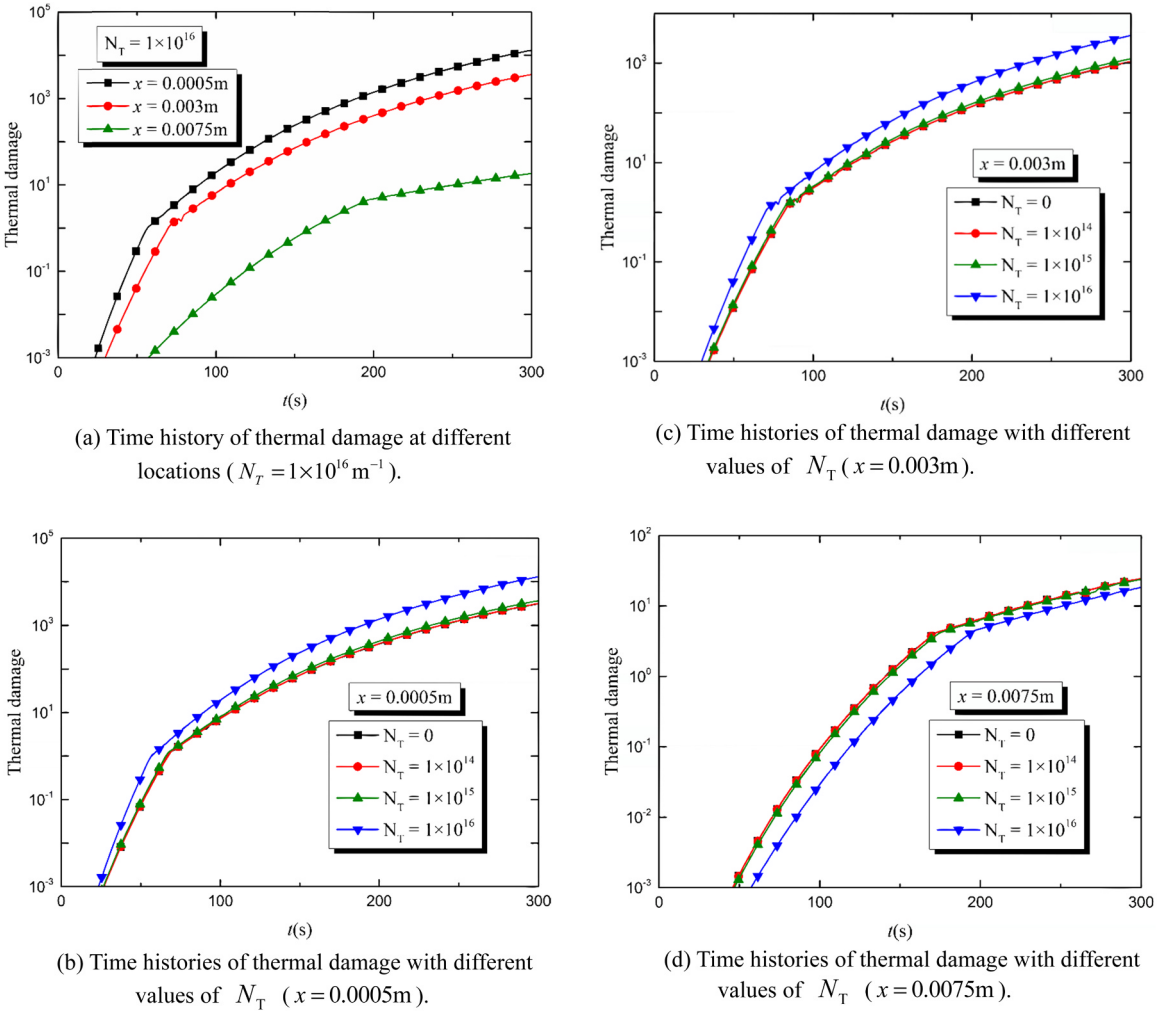

(a) Time history of thermal damage at different locations ($N_T = 1\times10^{16}\,\mathrm{m}^{-1}$).

(c) Time histories of thermal damage with different values of N_T ($x = 0.003\mathrm{m}$).

(b) Time histories of thermal damage with different values of N_T ($x = 0.0005\mathrm{m}$).

(d) Time histories of thermal damage with different values of N_T ($x = 0.0075\mathrm{m}$).

Fig. 7. Thermal damage variation with time.

irreversible thermal damage occurs earlier in the top two layers. However, it takes more time to irreversibly burn the subcutaneous tissue. These conclusions are in good agreement with Fig. 7. The embedding of the gold nanoshells can help concentrating the laser energy in the tumor instead of the subcutis. And the subcutaneous tissues will be protected from being burnt.

It is shown in Table 4 and Fig. 5 that the embedding of nanoshells can influence the energy distribution in the three-layered system by increasing the absorption coefficient of the tumor. This effect shows up when $N_T = 1 \times 10^{16} m^{-1}$ and becomes more and more obvious with the increasing of N_T. Fig. 8(a) shows the thermal damage variation with the volumetric density of the gold nanoshells in each layer. The thermal damage parameters in skin and tumor increase with the increment of the nanoshell volumetric density. However the thermal damage in the subcutis decreases with the increment of the nanoshell density, which can also be found in Fig. 8(b)-(d). The thermal damage is influenced by the thermal characteristics, the radiation time and the energy power of the laser source. With the assistance of the gold nanoshells, it is easier to ensure the safety of the subcutis during the humor thermal treatment by adjusting the volumetric density of the nanoshells, the radiation duration and the energy power of the laser source.

As is introduced in Section 4, the thermal damage can be classified into three degrees according to the parameter Ω. In order to embody the burn depths in the three layers more intuitively, the variations of the burn depth in the target tissue are shown in Fig. 9. The thermal damage in bio-tissue is caused by the heat accumulation and the duration of the thermal effect is an important factor on the burn. The degree of thermal damage increases as time passes, so the burn depths in three degrees all increase with time, which can be found from Fig. 9(a). Fig. 9(b) shows the variation of burn depth with the nanoshell volumetric density. With the increment of the nanoshell

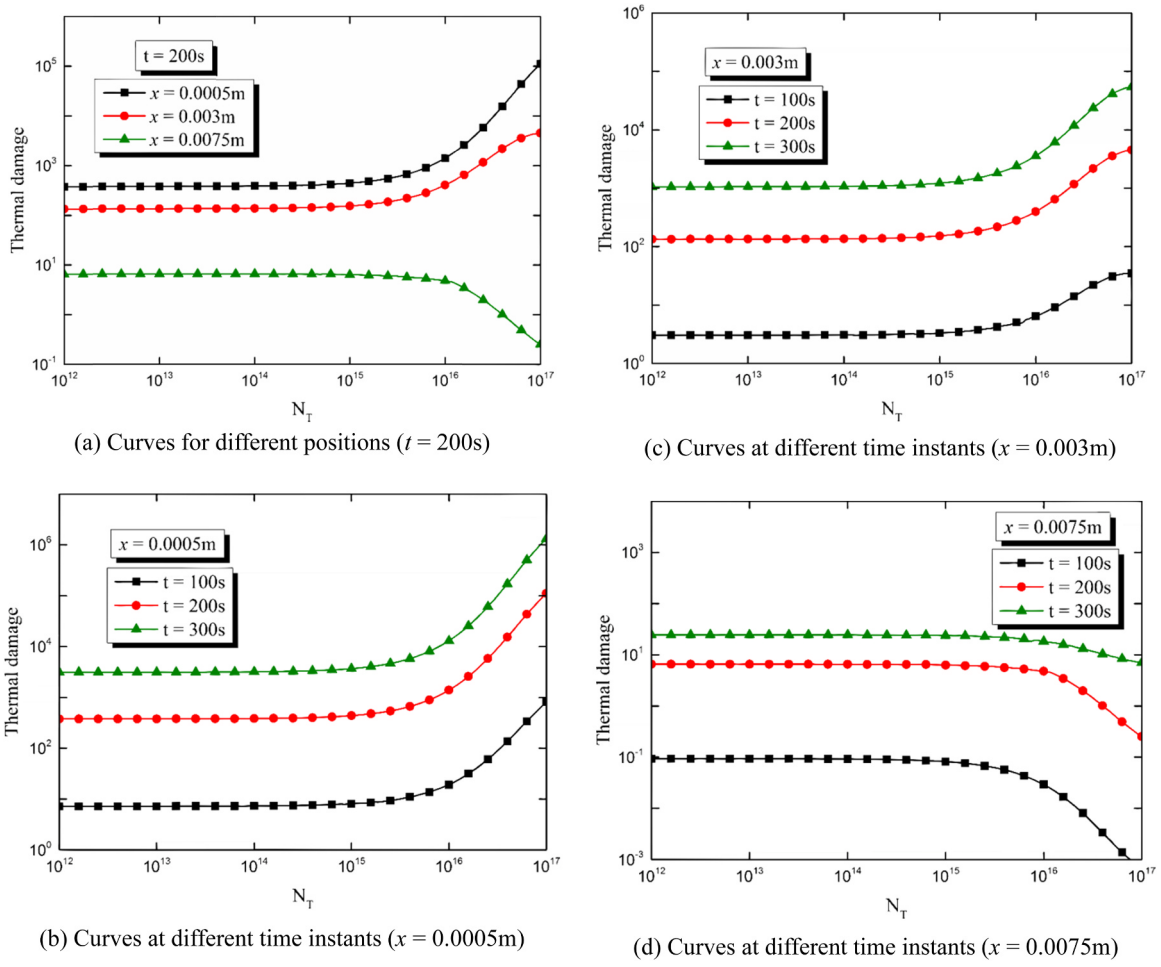

Fig. 8. Thermal damage variation with the volumetric density of the gold nanoshells.

density, the temperature increases in the rumor layer while decreases in the subcutis. As a result, the thermal damage in the tumor becomes more serious and the burnt region is smaller. As is shown in Fig. 9(b), when the nanoshell density N_T increases to a proper value, the burnt region in subcutis begins to decrease and the serious burn (the third-degree burn) starts to appear in the tumor. It comes to a conclusion that the gold nanoshells can be used to improve the tumor-killing effects and reduce the thermal damage to the healthy subcutis.

6. Conclusions

Thermal treatment is an efficient therapy method for tumor because the tumor cells are more sensitive to high temperature than the healthy cells are. In the present study, the thermal response of the bio-tissue in the nanoshell-assisted thermal treatment for the subcutis tumor was investigated. The target tissue was simplified as a one-dimensional model, which is composed of three layers: skin, tumor and subcutaneous tissue. Gold nanoshells were embedded in the tumor to augment its optical absorption property. A continuous laser beam irradiated on the top surface of the model. The governing equations were analytically solved with the usage of Green's function method. The thermal responses of the target tissue, including the temperature distribution and the thermal damage distribution, were derived.

The embedding of the gold nanoshells can increase the absorption coefficient of the tumor, which means that more energy is absorbed by the tumor and less by the subcutaneous tissue. By selecting the proper volumetric density of the nanoshells, the high-temperature zone can be limited in the tumor instead of the subcutis and the serious burn will occur mainly in tumor with proper irradiation duration. Embedding gold nanoshell is an effective assistance in the thermal treatment for subcutis tumor. The therapeutic efficiency can be increased and the subcutaneous tissue can be well protected from thermal damage. The analytical solution for the thermal response of the bio-tissue in the thermal treatment can help to determine the nanoshell volumetric density and the treatment duration.

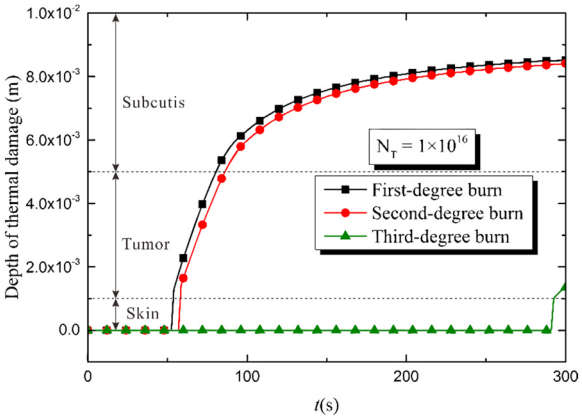

(a) Variation of thermal damage depth with time.

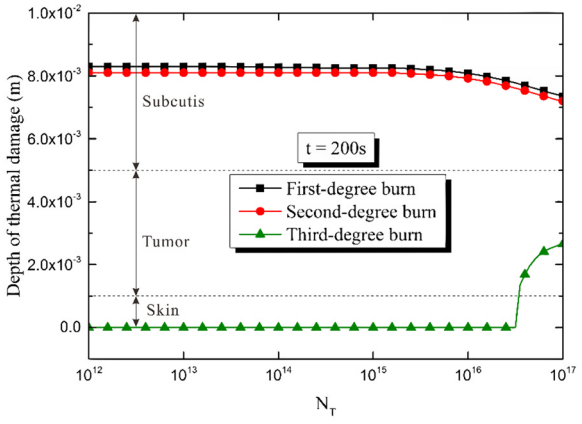

(b) Variation of thermal damage depth with N_T.

Fig. 9. Variation of thermal damage depth in the target tissue.

Acknowledgements

This work is financially supported by the National Natural Science Foundation of China under grant number 11872098 and the Academic Excellence Foundation of BUAA for PhD Students. The authors would like to gratefully acknowledge the support.

Conflict of interest

The authors declare that they have no conflict of interest.

Funding

This work was supported by the National Natural Science Foundation of China [grant number 11872098] and the Academic Excellence Foundation of BUAA for PhD Students.

References

Afrin, N., Zhou, J.H., Zhang, Y.W., Tzou, D.Y., Chen, J.K., 2012. Numerical simulation of thermal damage to living biological tissues induced by laser irradiation based on a generalized dual phase lag model. Numer. Heat Transf. Part A-Appl. 61, 483–501.
Cercadillo-Ibarguren, I., Espana-Tost, A., Arnabat-Dominguez, J., Valmaseda-Castellon, E., Berini-Aytes, L., Gay-Escoda, C., 2010. Histologic evaluation of thermal damage produced on soft tissues by CO_2, Er,Cr:YSGG and diode lasers. Med. Oral Patol. Oral Cirugia Bucal 15, E912–E918.
Cui, Y., Li, Y.H., Xing, Y.F., Yang, T.Z., Song, J.H., 2016. One-dimensional thermal analysis of the flexible electronic devices integrated with human skin. Micromachines 7.
Dai, W.Z., Yu, H.F., Nassar, R., 2004. A fourth-order compact finite-difference scheme for solving a 1-D Pennes' bioheat transfer equation in a triple-layered skin structure. Numer. Heat Transf. Part B-Fundam. 46, 447–461.
Ezzat, M.A., AlSowayan, N.S., Al-Muhiameed, Z.I.A., Ezzat, S.M., 2014. Fractional modelling of Pennes' bioheat transfer equation. Heat Mass Transf. 50, 907–914.
Flint, T.F., Francis, J.A., Smith, M.C., Vasileiou, A.N., 2018. Semi-analytical solutions for the transient temperature fields induced by a moving heat source in an orthogonal domain. Int. J. Therm. Sci. 123, 140–150.
Hatef, A., Fortin-Deschenes, S., Boulais, E., Lesage, F., Meunier, M., 2015. Photothermal response of hollow gold nanoshell to laser irradiation: Continuous wave, short and ultrashort pulse. Int. J. Heat Mass Transf. 89, 866–871.
Hooshmand, P., Moradi, A., Khezry, B., 2015. Bioheat transfer analysis of biological tissues induced by laser irradiation. Int. J. Therm. Sci. 90, 214–223.
Huang, C.J., Chu, S.H., Li, C.H., Lee, T.R., 2016. Surface modification with zwitterionic cysteine betaine for nanoshell-assisted near-infrared plasmonic hyperthermia. Colloids Surf. B-Biointerfaces 145, 291–300.
Huang, X.H., Jain, P.K., El-Sayed, I.H., El-Sayed, M.A., 2008. Plasmonic photothermal therapy (PPTT) using gold nanoparticles. Lasers Med. Sci. 23, 217–228.
Kumar, D., Rai, K.N., 2016. A study on thermal damage during hyperthermia treatment based on DPL model for multilayer tissues using finite element Legendre wavelet Galerkin approach. J. Therm. Biol. 62, 170–180.
Lin, S.M., 2013. Analytical solutions of bio-heat conduction on skin in Fourier and non-Fourier models. J. Mech. Med. Biol. 13.
Lin, S.M., Li, C.Y., 2016. Analytical solutions of non-Fourier bio-heat conductions for skin subjected to pulsed laser heating. Int. J. Therm. Sci. 110, 146–158.
Liu, C.H., Mi, C.C., Li, B.Q., 2009. Transient temperature response of pulsed-laser-induced heating for nanoshell-based hyperthermia treatment. Ieee Trans. Nanotechnol. 8, 697–706.
Liu, K.C., Wang, Y.N., Chen, Y.S., 2012. Investigation on the bio-heat transfer with the dual-phase-lag effect. Int. J. Therm. Sci. 58, 29–35.
Ma, J.X., Sun, Y.X., Yang, J.L., 2017. Analytical solution of non-Fourier heat conduction in a square plate subjected to a moving laser pulse. Int. J. Heat Mass Transf. 115, 606–610.
Ma, J.X., Sun, Y.X., Yang, J.L., 2018. Analytical solution of dual-phase-lag heat conduction in a finite medium subjected to a moving heat source. Int. J. Therm. Sci. 125, 34–43.
Malek, A., Abbasi, G., 2016. Optimal control for Pennes' bioheat equation. Asian J. Control 18, 674–685.
Moritz R, H.F.C., 1947. Studies of thermal injury II: the relative importance of time and surface temperature in the causation of cutaneous burns. Am. J. Pathol. 23 (5), 695–720.
Nobrega, S., Coelho, P.J., 2017. A parametric study of thermal therapy of skin tissue. J. Therm. Biol. 63, 92–103.
Orndorff, C., Ponomarev, S., Dai, W.Z., Bejan, A., 2017. Thermal analysis in a triple-layered skin structure with embedded vasculature, tumor, and gold nanoshells. Int. J. Heat Mass Transf. 111, 677–695.
Ozisik, M.N., 1980. Heat Conduction. John Wiley & Sons, Inc, New York.
Pennes, H., 1948. Analysis of tissue and arterial blood temperatures in the resting human forearm. J. Appl. Physiol. 93–122.
Shih, T.C., Yuan, P., Lin, W.L., Kou, H.S., 2007. Analytical analysis of the Pennes bioheat transfer equation with sinusoidal heat flux condition on skin surface. Med. Eng. Phys. 29, 946–953.
Sun, Y.X., Ma, J.X., Liu, S.B., Yang, J.L., 2017. Analytical solution of transient heat conduction in a bi-layered circular plate irradiated by laser pulse. Can. J. Phys. 95, 322–330.
Tang, X.G., Dai, W.Z., Nassar, R., Bejan, A., 2006. Optimal temperature distribution in a three-dimensional triple-layered skin structure embedded with artery and vein vasculature. Numer. Heat Transf. Part A-Appl. 50, 809–834.
Tjahjono, I.K., Bayazitoglu, Y., 2008. Near-infrared light heating of a slab by embedded nanoparticles. Int. J. Heat Mass Transf. 51, 1505–1515.
Tuncer, I., Ozcakir-Tomruk, C., Sencift, K., Cologlu, S., 2010. Comparison of conventional surgery and CO_2 laser on intraoral soft tissue pathologies and evaluation of the collateral thermal damage. Photomed. Laser Surg. 28, 75–79.
Tzou, D.Y., 1995. A unified field approach for heat conduction from macro- to micro-scales. J. Heat Transf. 117, 8–16.
Vahidhosseini, S.M., Barati, E., Esfahani, J.A., 2016. Green's function method (GFM) and mathematical solution for coupled equations of transport problem during convective drying. J. Food Eng. 187, 24–36.
Vera, J., Bayazitoglu, Y., 2009a. Gold nanoshell density variation with laser power for induced hyperthermia. Int. J. Heat Mass Transf. 52, 564–573.
Vera, J., Bayazitoglu, Y., 2009b. A note on laser penetration in nanoshell deposited tissue. Int. J. Heat Mass Transf. 52, 3402–3406.
Verma, A.K., Rath, P., Mahapatra, S.K., 2017. Assessment of thermal damage during skin tumor treatment using thermal wave model: a realistic approach. J. Heat Transf.-Trans. Asme 139, 051102–1 - 051102-9.
Xu, X.A., Meade, A., Bayazitoglu, Y., 2011. Numerical investigation of nanoparticle-assisted laser-induced interstitial thermotherapy toward tumor and cancer treatments. Lasers Med. Sci. 26, 213–222.
Yen, D.H.Y., Beck, J.V., 2004. Green's functions and three-dimensional steady-state heat-conduction problems in a two-layered composite. J. Eng. Math. 49, 305–319.
Yue, K., Zhang, X.X., Yu, F., 2004. An analytic solution of one-dimensional steady-state Pennes' Bioheat transfer equation in cylindrical coordinates. J. Therm. Sci. 13, 255–258.
Zhou, J.H., Chen, J.K., Zhang, Y.W., 2009. Dual-phase lag effects on thermal damage to biological tissues caused by laser irradiation. Comput. Biol. Med. 39, 286–293.